Effects of Active Site Mutations on the Metal Binding Affinity, Catalytic Competence, and Stability of the Family II Pyrophosphatase from *Bacillus subtilis*†

Pasi Halonen,‡,§ Marko Tammenkoski,‡ Laila Niiranen,‡ Sauli Huopalahti,‡ Alexey N. Parfenyev,| Adrian Goldman,+ Alexander Baykov,*,| and Reijo Lahti*,‡

Department of Biochemistry, University of Turku, FIN-20014 Turku, Finland, A. N. Belozersky Institute of Physico-Chemical Biology and School of Chemistry, Moscow State University, Moscow 119899, Russia, and Structural Biology and Biophysics, Institute of Biotechnology, University of Helsinki, FIN-00014 Helsinki, Finland

Received September 24, 2004; Revised Manuscript Received December 5, 2004

ABSTRACT: Family II inorganic pyrophosphatases (PPases) have been recently found in a variety of bacteria. Their primary and tertiary structures differ from those of the well-known family I PPases, although both have a binuclear metal center directly involved in catalysis. Here, we examined the effects of mutating one Glu, four His, and five Asp residues forming or close to the metal center on Mn^{2+} binding affinity, catalysis, oligomeric structure, and thermostability of the family II PPase from *Bacillus subtilis* (*bs*PPase). Mutations H9Q, D13E, D15E, and D75E in two metal-binding subsites caused profound (10^4- to 10^6-fold) reductions in the binding affinity for Mn^{2+}. Most of the mutations decreased k_{cat} for $MgPP_i$ by 2−3 orders of magnitude when measured with Mn^{2+} or Mg^{2+} bound to the high-affinity subsite and Mg^{2+} bound to both the low-affinity subsite and pyrophosphate. In the E78D variant, the k_{cat} for the Mn-bound enzyme was decreased 120-fold, converting *bs*PPase from an Mn-specific to an Mg-specific enzyme. K_m values were less affected by the mutations, and, interestingly, were decreased in most cases. Mutations of His^{97} and His^{98} residues, which lie near the subunit interface, greatly destabilized the *bs*PPase dimer, whereas most other mutations stabilized it. Mn^{2+}, in sharp contrast to Mg^{2+}, conferred high thermostability to wild-type *bs*PPase, although this effect was reduced by all of the mutations except D203E. These results indicate that family II PPases have a more integrated active site structure than family I PPases and are consequently more sensitive to conservative mutations.

Soluble inorganic pyrophosphatase (PPase,[1] EC 3.6.1.1) is an essential enzyme catalyzing the cation-dependent interconversion of inorganic pyrophosphate and orthophosphate. This reaction provides a thermodynamic pull for many biosynthetic reactions (*1, 2*) and is essential for life (*3*−*5*). Soluble PPases are classified into two families based on their amino acid sequences and tertiary structures. Family I includes both bacterial and eukaryotic PPases of which the PPases of *Escherichia coli* and *Saccharomyces cerevisiae* are the most extensively characterized members (*6*−*11*). Family II was discovered only recently (*12, 13*) and has not yet been studied in detail. All known family II PPases come from prokaryotic organisms and are homodimers of ∼34 kDa subunits (*14*) that consist of two clearly defined domains (*15, 16*).

All PPases require divalent cations for activity. The mechanism of PP_i hydrolysis by family I PPases involves the attack of a water molecule/hydroxide activated by a binuclear metal center on the electrophilic phosphoryl group, also activated by this metal center and a third metal ion, coming with substrate, to yield a pentavalent intermediate (*17*). Although family I and II PPases share no overall structural similarity, the identity of key amino acid residues and the positions of activating metal ions in their active sites are very similar, possibly reflecting conservation of the catalytic mechanism (*15, 16*). However, the two families differ remarkably in their preference for activating cation: Mg^{2+} is the best cofactor for family I, and Mn^{2+} is the best for family II. Although the activities of family I and II PPases are similar with Mg^{2+} as the cofactor, family II PPases have 10- to 20-fold greater activity when Mn^{2+} is the cofactor. Cations, especially Mn^{2+}, also promote dimerization of the family II type PPases (*14*). The overwhelming preference for Mn^{2+} over Mg^{2+} in family II enzymes is thought to be due to the presence of histidine residues at the enzyme active site, residues that are not found in family I PPases (*15*). However, to date no detailed analysis has been conducted to elucidate how the active site residues in family II PPases

† This work was supported by The Academy of Finland Grants 201611, 172168, and 178376, ISB (The National Graduate School in Informational and Structural Biology)/ the Ministry of Education and the Academy of Finland, The Sigrid Juselius Foundation, The Russian Foundation for Basic Research Grant 03-04-48798, and The Ministry of Industry, Science, and Technologies of the Russian Federation 1706−2003−4.

* To whom correspondence should be addressed. R.L.: tel, 358-2-3336845; fax, 358-2-3336860; e-mail, reijo.lahti@utu.fi. A.A.B.: tel, 7-095-9395541; fax, 7-095-9393181; e-mail, baykov@genebee.msu.su.

‡ University of Turku.

§ Current address: VTT Biotechnology, P.O. Box 1500, FIN-02044 VTT.

| Moscow State University.

+ University of Helsinki.

[1] Abbreviations: *bs*PPase, *Bacillus subtilis* inorganic pyrophosphatase; CD, circular dichroism; P_i, orthophosphate; PP_i, pyrophosphate; PPase, inorganic pyrophosphatase; TES, 2-{[2-hydroxy-1,1-bis(hydroxymethyl)ethyl]amino}ethanesulfonic acid.

10.1021/bi047926u CCC: $30.25 © 2005 American Chemical Society
Published on Web 02/12/2005

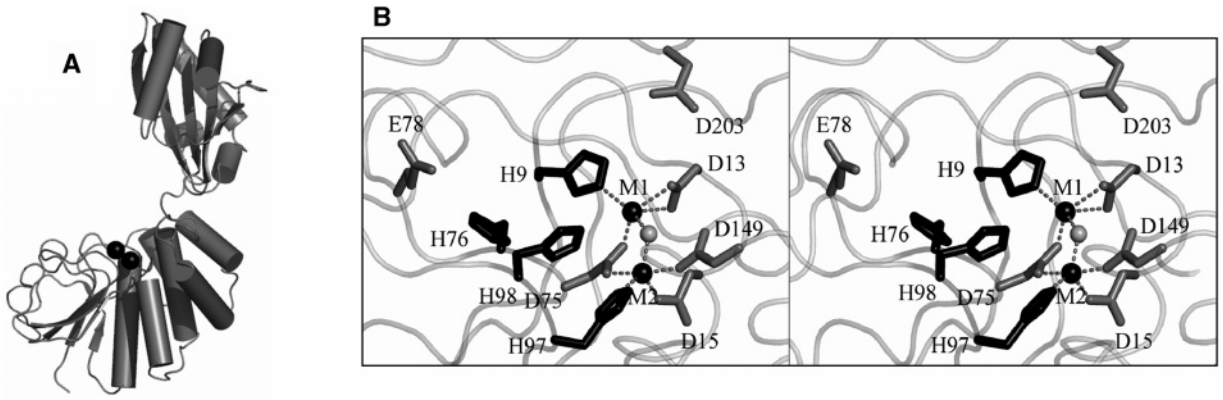

FIGURE 1: Structure of *B. subtilis* PPase monomer in an open conformation (*16*; PDB code 1K23). (A) Ribbon diagram showing the C- and N-terminal domains (top and bottom, respectively), which are connected by an eight-residue interdomain linker. The metals at the binding subsites M1 and M2 are shown as small spheres. (B) Stereoview of the active site at the domain interface showing the residues that were selected for mutation in the present study. The Mn^{2+} ions at the binding subsites M1 and M2 are shown as black spheres, the bridging water molecule appears as a gray sphere, the negatively charged conserved residues (four aspartates and one glutamate) are shown in gray, and histidines are shown in black. The figures were created with PyMOL (*18*).

actually affect cation specificity, quaternary structure, and PP_i hydrolysis, and thus, the molecular basis of the differences between families I and II has remained unresolved.

The tertiary structure of *B. subtilis* PPase monomer in an open conformation is shown in Figure 1A. The N-terminal domain (residues 1−188) contains the metal binding subsites (denoted M1 and M2) where the binding of Mn^{2+} and, to a lesser degree Mg^{2+}, activates the enzyme toward PP_i hydrolysis and stimulates dimerization. The C-terminal domain (residues 196−309) contains basic residues (Lys^{205}, Arg^{295}, and Lys^{296}) that participate in substrate and product binding (*15, 16*). The active site is thus formed at the interface between the N- and C-terminal domains when they move closer to each other upon substrate or product binding (*15, 16*). This can be easily accomplished in response to substrate binding because the domains are connected by a flexible hinge. These structural features in family II PPases endow the active site with high dynamic flexibility.

In the present study we used site-directed mutagenesis in combination with functional studies of the mutant PPases to elucidate the role of active site residues in metal binding, catalysis, dimerization, and stability of family II PPase from *B. subtilis* (*bs*PPase). The metal binding subsites M1 and M2 and the residues in the N-terminal domain chosen for mutation are shown in Figure 1B. Aspartates 13, 15, 75, and 149 and histidines 9 and 97, which are conserved among the family II PPases, are direct ligands to the two metal ions in the holoenzyme structure (*15, 16*). His76, Glu78, and His98 are also conserved, but because they are oriented away from the metal binding subsites, their exact role in catalysis is unknown. A conserved aspartate at position 203 in the C-terminal domain, believed to take part in substrate binding, was also included in the present study. Our rationale for the site-directed mutagenesis was to conserve either the charge (D → E and E → D substitution) or the shape (H → Q) of the residue, thus minimizing drastic structural changes.

EXPERIMENTAL PROCEDURES

Enzyme. Site-directed mutagenesis was performed with a QuickChange mutagenesis kit (Stratagene, La Jolla, CA). *Escherichia coli* C43(DE3) was transfected with a plasmid containing *ppa* gene encoding *bs*PPase or a variant, and the enzyme was expressed and purified as described previously (*14*). All preparations of the wild-type and variant proteins were >95% homogeneous, according to SDS−PAGE analysis, and completely free of *E. coli* PPase. Metal cofactors (10 mM $MnCl_2$ and 15 mM $MgCl_2$) were added to all purification buffers to stabilize the native enzyme structure. The purified enzyme stock (20−50 mg/mL) contained 0.15 M Tris-HCl, pH 7.2, 10 mM $MnCl_2$, and 15 mM $MgCl_2$. To remove metals, dialysis was carried out for 2 days at 4°C against 0.1 M Tris-HCl, pH 7.2 containing 2 mM EDTA, followed by three cycles of dilution and concentration in 83 mM TES−KOH, pH 7.2, 17 mM KCl, and 50 μM EGTA using a Centricon YM-10 device (Amicon Bioseparations, Millipore Corporation, Bedford, MA). Protein concentrations were determined on the basis of the extinction coefficient ($\epsilon_{280}^{1\%} = 2.64$) calculated from the amino acid composition and using ProtParam (http://expasy.pku.edu.cn/tools/protparam.html). The value of the extinction coefficient was confirmed by direct measurement of the absorbance of a solution prepared from dried and weighed enzyme (*14*). Alternatively, we measured the protein concentration using the Bradford method (*19*) standardized against the above PPase protein extinction coefficient.

Sedimentation. Analytical ultracentrifugation was carried out in a Spinco E instrument (Beckman Instruments, Palo Alto, CA) with scanning at 280 nm. The samples contained 26 μM enzyme and 1.5 mM $MnCl_2$ or $MgCl_2$ in 83 mM TES−KOH, 17 mM KCl, pH 7.2. Before each run, the samples were incubated for 2−3 h at 25 °C. The sedimentation velocity was measured at 48,000 rpm, and the sedimentation coefficient, $s_{20,w}$, was calculated as described by Chervenka (*20*).

Equilibrium Dialysis. Mn^{2+} binding was assayed by equilibrium microdialysis with a more than 100-fold excess of dialysis buffer compared to enzyme solution. The initial enzyme concentration was 0.4 mM. The amounts of free and bound Mn^{2+} were measured by atomic absorption spectroscopy at 279.5 nm (*14*).

Thermal Unfolding. Temperature-induced unfolding was measured by circular dichroism (CD) on a Jasco-720 spectropolarimeter equipped with a PTC-38WI Peltier-type temperature control by monitoring $\Delta\theta_{222}$ (change in ellipticity

Table 1: Measured Parameter Values for Wild-type and Variant *bs*PPases[a]

		$s_{20,w}$ (S)[b]			k_{cat} (s^{-1})[c]		K_m (μM)[c]		T_m (°C)[d]		
variant	binding site	Mn	Mg	K_{Mn} (μM)	Mn	Mg	Mn	Mg	Mn	Mg	EDTA
WT[e]		4.0	3.5	0.005 ± 0.002	3120 ± 70	160 ± 10	160 ± 10	29 ± 11	≥ 80	50	46
H9Q	M1	4.2	4.3	2000 ± 300	1.5 ± 0.1	0.59 ± 0.01	114 ± 39	3.6 ± 0.3	54	nd[f]	nd
D13E	M1	4.2	3.5	20 ± 4.8	11.6 ± 0.4	1.9 ± 0.1	121 ± 12	8.1 ± 2.4	58/69	44	42
D15E	M2	4.1	3.9	9.5 ± 2.2	9.6 ± 0.6	0.75 ± 0.01	140 ± 18	1.8 ± 0.1	67	45	49
D75E	M1/M2	4.1	4.0	580 ± 50	6.1 ± 0.4	0.046 ± 0.003	64 ± 8	15 ± 6	71	47	46
H76Q		3.7	3.5	> 5000	1.6 ± 0.1	1.5 ± 0.1	1.6 ± 0.2	3.4 ± 0.7	59	nd	nd
E78D		3.9	3.8	0.002 ± 0.0010	27 ± 1	163 ± 17	67 ± 9	99 ± 16	71	55	45
H97Q	M2	2.8	2.5	0.055 ± 0.016	13 ± 1	8.0 ± 0.8	37 ± 9	12 ± 4	69	47	45
H98Q		3.0	2.5	0.011 ± 0.005	1.1 ± 0.1	0.38 ± 0.01	81 ± 10	54 ± 7	62/70	48	nd
D149E	M2	4.1	3.9	0.030 ± 0.010	6.3 ± 0.3	1.50 ± 0.02	50 ± 9	2.9 ± 0.4	63/72	52	47
D203E		4.1	4.0	0.006 ± 0.002	1030 ± 40	120 ± 5	940 ± 70	406 ± 30	≥ 80	43	42

[a] Prior to measurements, enzymes were preincubated at room temperature at 26 μM (sedimentation), 0.4−1 mM (steady-state kinetics), or 5 μM (thermal unfolding) with 1.5 mM Mn^{2+}, 1.5 mM Mg^{2+}, or 2 mM EDTA for 2−3 h (sedimentation) or 24 h (other measurements). The enzyme concentration during measurements was 26 μM (sedimentation), 0.4 mM (equilibrium dialysis), or 5 μM (thermal unfolding). [b] The $s_{20,w}$ values are accurate to ±0.2 S. [c] The k_{cat} and K_m were determined in the presence of 20 mM Mg^{2+} as the cofactor. The K_m values were calculated as the total PP_i concentration. The k_{cat} and K_m values for the wild-type enzyme were taken from Parfenyev et al. (*14*). [d] The T_m values are accurate to ±1 °C. [e] WT, wild-type. [f] nd, no peak observed in the derivatized spectrum.

at 222 nm) with an averaging time of 16 s. The measurements were made in a quartz cuvette with a 0.1 cm optical path. Enzyme (5 μM) was incubated for 24 h with 1.5 mM Mn^{2+} or Mg^{2+} (producing the cation-activated enzyme species) or 2 mM EDTA (producing the cation-depleted form) in 21 mM TES−KOH, pH 7.2, containing 4 mM KCl and either 13 μM EGTA (Mn^{2+} experiment) or 130 μM EGTA (Mg^{2+} experiment).

Activity Measurements. The rates of PP_i hydrolysis were determined by continuously following the liberation of P_i into the reaction medium (*21*). The enzyme stock solution (0.4 to 1 mM) was preincubated for 24 h with 1.5 mM $MnCl_2$ or $MgCl_2$. Dilutions of the enzyme were prepared in the same medium just prior to PP_i hydrolysis measurements. PP_i hydrolysis was carried out in 83 mM TES−KOH, 17 mM KCl, pH 7.2 in the presence of 20 mM free Mg^{2+}. The rate of PP_i hydrolysis was measured as a function of the substrate concentration (calculated as the sum of $MgPP_i$ and Mg_2PP_i concentrations).

Calculations. The equilibrium dialysis data were fitted to eq 1, where *n* is the number of metal ions bound per subunit, [M] is free Mn^{2+} concentration, and K_{Mn} is the dissociation constant of the enzyme-metal complex. A dissociation constant of 6.3 nM for the Mn−EGTA complex at pH 7.2 was used to estimate the concentration of free Mn^{2+} in the presence of EGTA (*14*)

$$n = [M]/(K_{Mn} + [M]) \quad (1)$$

The mean residue ellipticity ([θ]) at 222 nm was calculated according to eq 2, where M_{MRW} is the mean weight of an amino acid residue (110.03 g/mol), *d* is the cell path in cm, and $[E]_t$ is enzyme concentration in mg/mL. The melting temperature for wild-type *bs*PPase and each variant was obtained by calculating the first derivative of the averaged CD spectra and identifying the maximum from the smoothed first derivative of the CD spectra

$$[\theta] = [\theta]_{222} M_{MRW} / 10 d [E]_t \quad (2)$$

All data analyses, equation fittings, and plot constructions were performed using Origin 6.0 (MicroCal, Microcal Software, Inc., Northampton, MA).

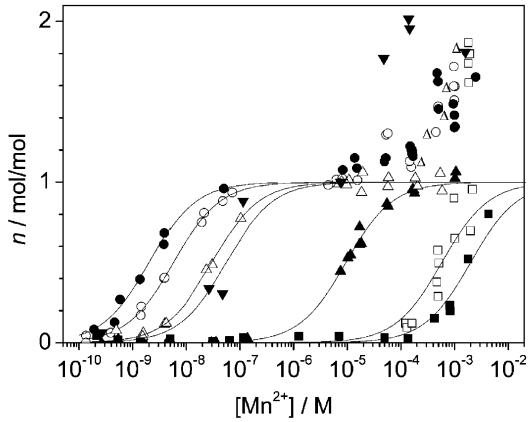

FIGURE 2: Mn^{2+} binding as measured by equilibrium microdialysis. Curves: wild-type *bs*PPase (○), H9Q (■), D15E (▲), D75E (□), E78D (●), H97Q (▼), and D149E (△). The data were fitted according to a one-binding site model (eq 1).

RESULTS

Quaternary Structure. To characterize the effects of the substitutions on quaternary structure stability, sedimentation coefficients ($s_{20,w}$) were measured in the presence of Mn^{2+} and Mg^{2+} at pH 7.2 (Table 1). At this pH value, 26 μM wild-type *bs*PPase gave $s_{20,w}$ values of 4.0 and 3.5 S in the presence of Mn^{2+} and Mg^{2+}, respectively. Therefore, the enzyme is entirely dimeric in the presence of Mn^{2+} and is a mixture of mostly dimer with some monomer in the presence of Mg^{2+} (*14*). Most variants used in this work had the same or slightly higher $s_{20,w}$ values (Table 1). Two notable exceptions were the H97Q and H98Q variants, which had $s_{20,w}$ values characteristic of a monomer in the presence of Mg^{2+} (2.5 S) and only slightly higher $s_{20,w}$ values in the presence of Mn^{2+} (Table 1).

Mn^{2+} Binding. We used equilibrium dialysis to measure Mn^{2+} binding to the variant *bs*PPases, as we have done previously for the wild-type enzyme (*14*). The dissociation constant K_{Mn}, which characterizes the binding of Mn^{2+} to the highest affinity site, was estimated in each case using only points corresponding to *n* (the number of metal ions bound per subunit) < 1.0 (Figure 2). Regardless of the affinity of the primary binding site, all variants, except H9Q and D15E, bound one additional metal ion in the presence

of millimolar concentrations of Mn^{2+}. However, we could not reliably measure differences between the variants for the weaker binding sites because at high Mn^{2+} concentrations the assay is less sensitive and Mn^{2+} may bind nonspecifically. The value of K_{Mn} reported for the D75E variant should be considered only a rough estimate, as this variant binds two metal ions with similar affinities.

As shown in Table 1, the affinities of the variants toward Mn^{2+} varied greatly (10^6-fold range in K_{Mn}), allowing them to be separated into three classes: tight binding (K_{Mn} in nanomolar range; E78D, H97Q, H98Q, D149E, and D203E), intermediate binding (K_{Mn} in micromolar range; D13E and D15E), and loose binding (K_{Mn} in millimolar range; H9Q, D75E, and H76Q) (Table 1).

Steady-State Kinetic Parameters. Values of k_{cat} and K_m for dimeric Mn and Mg forms of all variants were measured using 20 mM Mg^{2+} as the cofactor. To ensure that the enzymes remained dimeric during the assay, they were preincubated at high concentration (0.4−1 mM) in the assay buffer (without substrate), and dilution, where needed, was carried out immediately prior to each rate measurement. According to the above sedimentation data, most of the variants were expected to be dimers while in their stock solutions, although the H97Q and H98Q variants could be monomers. Earlier studies of wild-type *bs*PPase have shown that dimer-monomer interconversion proceeds slowly on the time scale of enzyme assay (*14*). Furthermore, only the initial linear portions of the P_i production curves were used to calculate the reaction rate, and the presence of a single enzyme form was consistent with linear Lineweaver−Burk plots.

As Table 1 makes clear, the k_{cat} decreased substantially (20−3600-fold) for both the Mn and Mg forms of the variants. The greatest effects on k_{cat} were found with the H9Q, H76Q, and H98Q variants (Mn-form) and the H9Q, D15E, D75E, and H98Q variants (Mg-form). Two notable exceptions were the D203E substitution (only a 1.3- to 3-fold decrease) and the E78D substitution, which decreased k_{cat} for the Mn-form 116-fold but had no effect on the Mg-form. As a result, the E78D variant was more active with Mg^{2+} bound than with Mn^{2+} bound. This was also reflected in the appearance of the time courses of PP_i hydrolysis by this variant (Figure 3). The time course curved upward when Mn-E78D was assayed in the presence of Mg^{2+}, indicating enzyme activation by slow displacement of the Mn^{2+} at the high affinity site with Mg^{2+} in the assay medium. In contrast, the P_i production curves for all other Mn^{2+}-preincubated variants curved downward as a result of a similar displacement, as previously reported for wild-type *bs*PPase (*14*). The time courses for the Mg^{2+}-preincubated enzymes were linear, as illustrated in Figure 3 for the E78D variant. Finally, the K_m values were much less affected by the substitutions and were decreased in most variants (Table 1), making them better catalysts in terms of K_m compared to the wild-type enzyme. The most striking example is the H76Q variant, with a 100-fold drop in K_m for the Mn-bound form. The decrease in K_m in the variants may be due to the decrease in the forward rate constant (reflected in k_{cat}) which contributes to K_m in the wild-type enzyme. By lowering k_{cat}, the variants more closely approach equilibrium kinetics.

*Thermal Unfolding.*The effect of active site substitutions on the structural integrity of *bs*PPase was characterized by

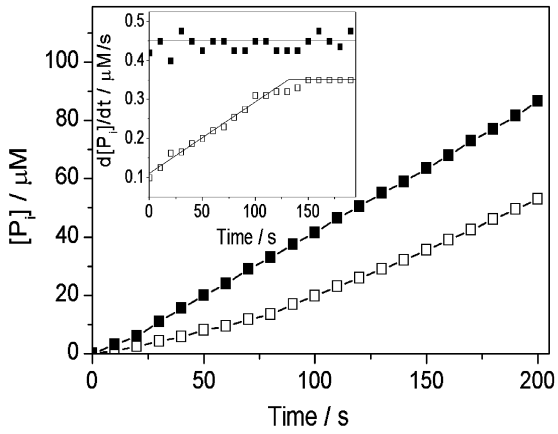

FIGURE 3: Time course of PP_i hydrolysis by the variant E78D preincubated with 1.5 mM Mg^{2+} (■) or Mn^{2+} (□). The assay mixture contained 57 μM PP_i, 20 mM $MgCl_2$, 40 μM EGTA, and 0.15 M Tris-HCl, pH 7.2. Inset: the first derivatives of the P_i production curves.

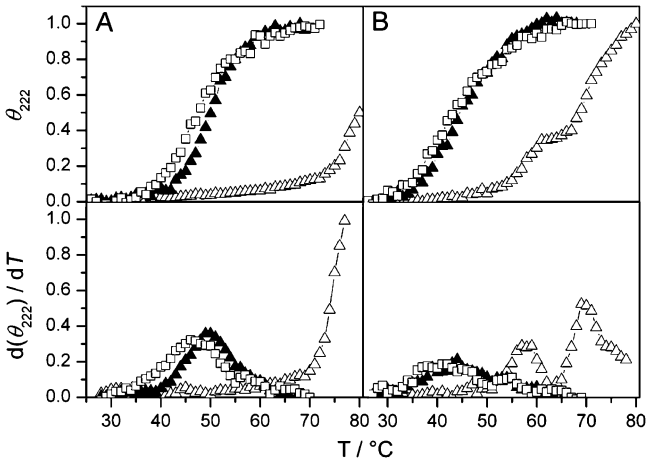

FIGURE 4: Measured θ_{222} vs temperature profiles (top) and their calculated first derivatives (bottom). Wild type *bs*PPase (A) and the variant D13E (B) were assayed in the absence of metal ions (□) or in the presence of 1.5 mM Mg^{2+} (▲) or Mn^{2+} (△).

measuring the molar ellipticity at 222 nm as a function of temperature. Our aim was to identify the residues essential for structural integrity and to estimate the degree of protection provided by cations against thermal denaturation. Unfortunately, thermal unfolding resulted in nonreversible denaturation of the enzymes, possibly because of aggregation and covalent modifications (*22*−*27*). Despite our efforts to obtain reversible thermal denaturation profiles, we could not find suitable buffer conditions, at least in the neutral pH region, for a detailed thermodynamic analysis of PPase stability. We therefore estimated the thermal stability of the apoenzymes and the protection provided by Mn^{2+} and Mg^{2+} ions from the melting temperature, T_m, defined as the temperature at the inflection point on the thermal denaturation curve and identified as the peak in a plot of the derivative of the CD spectra.

The thermal denaturation profiles (θ_{222} vs T) and the plots for the T_m determination ($d\theta_{222}/dT$ vs T) for the wild type *bs*PPase are shown in Figure 4A, and the respective data for the variant D13E are shown in Figure 4B. Because the thermal denaturation of wild-type Mn-*bs*PPase was less than 50% complete at 80 °C (Figure 4A), we could only estimate that its T_m was greater than 80 °C. Mg^{2+} ions, however,

provided far inferior protection against thermal denaturation ($T_m = 50$ °C), with a sigmoidal transition curve (Figure 4A, top), which reflects a high degree of cooperativity during denaturation. A highly cooperative denaturation profile with a T_m value of 47 °C was also obtained with the metal-depleted wild-type enzyme. The θ_{222} versus T profile for the D13E variant in the presence of Mn^{2+} exhibited an intermediate plateau (Figure 4B, top), leading to two peaks in the plot of the derivative of the CD spectrum (Figure 4B, bottom) and, consequently, two melting temperatures. Two clearly separated peaks on the plots of the derivative of the CD spectrum, indicating T_m values separated by approximately 9 °C, were also observed for variants D149E and H98Q in the presence of Mn^{2+} ions.

The T_m values estimated in the presence and absence of metal ions are summarized in Table 1. In the presence of Mn^{2+}, wild-type *bs*PPase was by far more stable than any variant except, perhaps, D203E. The lowest T_m values were observed with the variants H9Q and H76Q (a decrease of ≥ 26 °C and ≥21 °C, respectively), suggesting that a conformational change occurred. Interestingly, the T_m values of the Mg^{2+}-bound or metal-depleted enzyme were much less affected by the substitutions, and one variant (E78D) exhibited a significantly greater T_m value with Mg^{2+} than in the metal-depleted form. Furthermore, the melting temperatures could not be estimated with Mg^{2+} or without any metal ion for the H9Q and H76Q variants because the signal was too low to be discerned from the noise, suggesting that these variants may not have a single conformation.

DISCUSSION

Family II PPases are typical Mn-metalloenzymes that can and, most likely, do use other divalent cations as cofactors in vivo. Three metal ions per active site are required for catalysis, and two of them are organized into a binuclear center in the resting enzyme (*15*, *16*). Although the binding sites for the two metal ions in the binuclear center are structurally very similar, only one metal ion per subunit is bound with an affinity characteristic of metalloenzymes (*14*), probably because of electrostatic repulsion between the two closely separated metal ions. In addition to being indispensable for catalysis, the tightly bound metal ion greatly (over 10^5-fold) stimulates dimerization of PPase, which further enhances its catalytic efficiency. Family II PPases thus use cations in multiple ways to promote catalysis. Together, there are six conserved amino acid residues (four Asp and two His) that participate in binding the two metal ions in the PPase active site. The third metal ion has no protein ligands in the enzyme−substrate complex (*15*) and apparently binds with PP_i.

In the current report, we show how the interactions of the conserved residues with cations affect the structural organization, stability, and catalytic efficiency of family II PPases. Conserved active site Asp, Glu, and His residues that do not directly interact with metal ions were also included in this study. We found that most of the conservative mutations chosen had little effect on the overall structure of *bs*PPase, as shown by the lack of significant changes in the thermostability of the apo- and Mg-enzymes. However, most of the mutations caused profound changes in the metal binding and catalytic properties of *bs*PPase.

Metal Binding Determinants. Mutations of almost any ligand in either subsite (M1 or M2) of the binuclear metal center decreased metal binding affinity, as characterized by the parameter K_{Mn}; however the size of the effect varied from 6-fold (D149E) to $4 \cdot 10^5$-fold (H9Q) (Table 1). Interestingly, mutations in subsite M1 (H9Q and D13E) had greater effects than those in subsite M2 (D15E, H97Q and D149E), although recent metal binding studies by our group (*28*) showed that M2 binds Mn^{2+} first. Mutation of Asp75, which is common to M1 and M2, had a very large effect on K_{Mn} (a 10^5-fold increase). Moreover, mutation of the nearby His76 residue had an even greater effect ($>10^6$-fold). These findings indicate that the binuclear center has a highly integrated structure, such that distortion of any of its constituting residues affects the entire center. This hypothesis is supported by our observation that all of the mutations studied caused drastic decreases in k_{cat} (Table 1).

This behavior is in sharp contrast to that observed in family I PPases, in which the M1 and M2 subsites behave as relatively independent entities (*29*, *30*). Accordingly, mutations have much smaller and more localized effects in family I PPases compared to family II PPases. For example, mutations of M1 in *E. coli* PPase had practically no effect on M2 and vice versa (*29*), and mutation of M2 in *S. cerevisiae* PPase had no effect on M1 (*30*). This difference between family I and II PPases can be explained by considering the distance between the metal ions in the binuclear center; specifically, the metal ions in family II PPases are only 3.6 Å apart, and they are separated by only a single shared water molecule (*15*, *16*), whereas in family I PPases the metal ions are 4.9 Å apart, and the water bridge is comprised of two water molecules in the absence of phosphoryl ligand (*17*). These structural features make the metal binding sites in family I PPases more flexible and tolerant of ligand substitutions.

Dependence of the Subunit Interface on the Active Site. The subunit interface of *bs*PPase is formed by β-strand 6, and the loop between β-strands 5 and 6 from each subunit (residues 99−115) (*16*). Dimer stability strongly depends on the metal ion bound at the high affinity site. Thus, at the enzyme concentration used in the sedimentation experiments (26 μM), wild-type Mn-*bs*PPase is completely dimeric, Mg-*bs*PPase is predominantly dimeric, and apo-*bs*PPase is predominantly monomeric (*14*). None of the active site residues are at the subunit interface, but, as shown by the sedimentation experiments, the active site mutations had various effects on dimerization (Table 1).

First, the H97Q and H98Q mutations abolish dimerization in Mg-*bs*PPase and greatly reduce it in Mn-*bs*PPase. The reduced dimer stability of the H97Q and H98Q variants may be due to the fact that the mutated residues flank the dimer interface (residues 99−115). The imidazole group of His^{97} forms a hydrogen bond to Asp^{75} and a coordination bond to the metal at M2, whereas the imidazole group of His^{98} is hydrogen bonded to Asp^{96}. Disrupting these interactions appears to profoundly distort the structure of the interfacial segment.

Second, the H9Q, D75E, and H76Q mutations abolish the metal ion dependence of dimerization and greatly stimulate dimerization by the metal-free enzyme. Indeed, despite the very weak binding affinity for Mn^{2+} (and possibly Mg^{2+}),

which is not sufficient to affect the dimer-monomer equilibrium when 1.5 mM metal ions are present, the corresponding variants are completely or predominantly dimeric. Conversely, monomeric H97Q and H98Q variants bind Mn^{2+} almost as strongly as the dimeric wild-type enzyme, although dissociation of wild-type dimers decreases the binding affinity for Mn^{2+} more than 10^5-fold (*14*). The lack of a requirement for metal binding for dimerization of the H9Q, D75E and H76Q variants suggests that the structural changes induced by these mutations in monomeric enzyme resemble those induced by metal binding. His9, Asp75 and HQ76 are further away from the dimer interface, but due to the integrated nature of the binuclear metal center, the effects of their mutations could be easily propagated there.

Finally, the $s_{20,w}$ values measured in the presence of Mg^{2+} are consistently higher in most variants than for the wild type enzyme, possibly reflecting increased dimer stability. An intriguing alternative is that the corresponding mutations stimulate formation of a more "open" conformation of enzyme subunit, consisting of two domains joined by a flexible linker (*15, 16*). X-ray crystallographic data indicate that family II PPases can adopt a variety of conformations—from "closed" to "open" (*15, 16, 31*).

Catalysis and Cofactor Specificity. Most of the mutations decreased k_{cat} by 2−3 orders of magnitude, demonstrating the importance of the mutated residues in catalysis. K_m values were less affected and in most cases decreased, making the enzyme a better catalyst in terms of K_m. A notable exception is the D203E substitution, which markedly increased K_m but had a small effect on k_{cat}, consistent with the proposed role for Asp^{203} in PP_i binding (*15, 16*).

Interestingly, Glu^{78} seems to determine the cofactor specificity of *bs*PPase because, in terms of k_{cat}, the E78D variant is 6 times more efficient with Mg^{2+} than with Mn^{2+} bound at subsite M1. This corresponds to a 120-fold decrease in the ratio $k_{cat,Mn}/k_{cat,Mg}$ compared to the wild-type enzyme (Table 1); Mn^{2+} is not a better activator for the E78D variant. This change in cofactor specificity results from decreased $k_{cat,Mn}$ and unchanged $k_{cat,Mg}$. Importantly, Glu^{78} is not a metal ligand, and the E78D variant binds Mn^{2+} even tighter than wild-type. In another variant, H76Q, $k_{cat,Mn}$ and $k_{cat,Mg}$ are similar, but this clearly results from the inability of this variant to bind Mn^{2+} (Table 1). Consequently, H76Q variant binds a full complement of Mg^{2+} ions in the assay mixture, irrespective of the metal ion used in the preincubation. Almost all the other mutations that retain the ability to bind Mn^{2+} also shift the cation specificity in favor of Mg^{2+}, as indicated by a smaller $k_{cat,Mn}/k_{cat,Mg}$ ratio compared to that of the wild type (Table 1); it should be noted, however, that these mutations cause reductions in both k_{cat} values. In D75E the ratio $k_{cat,Mn}/k_{cat,Mg}$ is increased 7-fold, but, again, both k_{cat} values are reduced.

Residues His^{97} and His^{98} of *bs*PPase (and the matching residues of other family II PPases) are part of the so-called DHH-motif, which has been strongly linked to a phosphoesterase function (*32*−*34*). Originally identified by Aravind and Koonin (*33*), the DHH family of phosphoesterases includes *Drosophila melanogaster* Prune protein, *S. cerevisiae* exopolyphosphatase, several exonucleases, and family II PPases. An internal hydrogen bond bridge is formed by the carboxylate oxygens of Asp^{96} to His^{98}: Oδ1 of Asp^{96} connects to Nδ1 of His^{98}, and Oδ2 of Asp^{96} connects to the backbone nitrogen of His^{98}. This bonding orients the first His residue in the DHH-motif toward the metal ion at subsite M2, allowing the binding of Nϵ2 from His^{97} to the metal ion and Oδ1 of Asp^{75}. Additionally, Nδ2 of His^{98} interacts with one of the sulfate oxygens corresponding to the bridging oxygen of PP_i. Ahn et al. (*16*) have suggested the hydrogen bonds formed within the DHH motif fix the orientation of His^{98} to act as a general acid catalyst by protonating the leaving group phosphate. The largest reduction in k_{cat} for the Mn^{2+}-activated H98Q mutant (over 2800-fold; Table 1) seems to be consistent with this proposed role for His^{98}. However, the pK_a of the acidic group responsible for the decline in k_{cat} for wild-type Mn-*bs*PPase with increasing pH is as high as 10 ± 0.3 (measured at 20 mM Mg^{2+}) and decreases insignificantly (to 9.6 ± 0.2) upon the H98Q mutation (data not shown). These results argue against His^{98} being a general acid catalyst. Further work is clearly needed to establish the role of this important residue in family II PPase.

Thermostability. Thermal inactivation studies have indicated that *bs*PPase becomes slightly more stable in the presence of Mg^{2+} and highly stable in the presence of Mn^{2+}. On the basis of the lower limit of T_m (≥ 80 °C), wild-type *bs*PPase is a true thermophilic enzyme in the presence of Mn^{2+}, but thermally mesotolerant with Mg^{2+}. Most of the active site mutations only slightly affected the T_m value for Mg-bound or metal-free enzyme (Table 1), but markedly reduced the stabilizing affect of Mn^{2+}. As the H9Q variant shows very large changes in metal binding, thermostability and dimerization, it may have undergone some slight but widespread conformational change. The identification of two distinct T_m values in the denaturation profiles for the D13E, D149E, and H98Q variants probably reflects dissociation first into monomers followed by unfolding of monomers. Alternatively, two domains may have different stabilities in these variants.

To sum up, our results indicate that the binuclear metal center, which forms the core of the active site in family II PPases, has a highly integrated structure that is very sensitive to conservative mutations. Through His97 and 98, this center is also integrated with the nearby subunit interface, allowing transfer of information between these two important regions. Possibly because of this highly intergrated structure, the effects of some mutations (H76Q and E78D) presented in this work cannot be explained based on the wild-type enzyme structure. Mn^{2+} binding was greatly weakened in the H76Q variant (not a metal ligand) but only slightly weakened in the H97Q variant (a direct metal ligand). Furthermore, the k_{cat} value was decreased with the E78D variant when Mn^{2+} was the activator, but not when Mg^{2+} was the activator. The three-dimensional structures of these interesting variants, currently under study, will help to explain this unusual behavior and provide a deeper insight into family II PPase mechanism.

ACKNOWLEDGMENT

We thank P. V. Kalmykov and N. N. Magretova for their help in sedimentation analyses and I. P. Fabrichniy for helpful discussions.

REFERENCES

1. Kornberg, A. (1962) On the metabolic significance of phosphorolytic and pyrophosphorolytic reactions, in *Horizons in Biochemistry* (Kasha, M., and Pullman, B. Eds.), p 251−264, Academic Press, New York.
2. Peller, L. (1976) On the free energy changes in the synthesis and degradation of nucleic acids, *Biochemistry 15*, 141−146.
3. Chen, J., Brevet, A., Formant, M., Leveque, F., Schmitter, J.-M., Blanquet, S., and Plateau, P. (1990) Pyrophosphatase is essential for growth of *Escherichia coli*, *J. Bacteriol. 172*, 5686−5689.
4. Lundin, M., Baltscheffsky, H., and Ronne, H. (1991) Yeast *PPA2* gene encodes a mitochondrial inorganic pyrophosphatase that is essential for mitochondrial function, *J. Biol. Chem. 266*, 12168−12172.
5. Sonnewald, U. (1992) Expression of *E. coli* inorganic pyrophosphatase in transgenic plants alters photoassimilate partioning, *Plant J. 2*, 571−581.
6. Baykov, A. A., Cooperman, B. S., Goldman, A., and Lahti, R. (1999) Cytoplasmic inorganic pyrophosphatases, *Prog. Mol. Subcell. Biol. 23*, 127−150.
7. Baykov, A. A., Fabrichniy, I. P., Pohjanjoki, P., Zyryanov, A. B., and Lahti, R. (2000) Fluoride effects along the reaction pathway of pyrophosphatase. Evidence for a second enzyme-pyrophosphate intermediate, *Biochemistry 39*, 11939−11947.
8. Belogurov, G. A., Fabrichniy, I. P., Pohjanjoki, P., Kasho, V., Lehtihuhta, E., Turkina, M. V., Cooperman, B. S., Goldman, A., Baykov, A. A., and Lahti, R. (2000) Catalytically important ionizations along the reaction pathway of yeast pyrophosphatase, *Biochemistry 39*, 13931−13938.
9. Zyryanov, A. B., Pohjanjoki, P., Kasho, V. N., Shestakov, A. S., Goldman, A., Lahti, R., and Baykov, A. A. (2001) The electrophilic and leaving group phosphates in the catalytic mechanism of yeast pyrophosphatase, *J. Biol. Chem. 276*, 17629−17634.
10. Heikinheimo, P., Tuominen, V., Ahonen, A.-K., Teplyakov, A., Cooperman, B. S., Baykov, A. A., Lahti, R., and Goldman, A. (2001) Towards a quantum-mechanical description of metal assisted phosphoryl transfer in pyrophosphatase, *Proc. Natl. Acad. Sci. U.S.A. 98*, 3121−3126.
11. Samygina, V. R., Popov, A. N., Rodina, E. V., Vorobyeva, N. N., Lamzin, V. S., Polyakov, K. M., Kurilova, S. A., Nazarova, T. I., and Avaeva, S. M. (2001) The structures of *Escherichia coli* inorganic pyrophosphatase complexed with Ca^{2+} or $CaPP_i$ at atomic resolution and their mechanistic implications, *J. Mol. Biol. 314*, 633−645.
12. Young, T. W., Kuhn, N. J., Wadeson, A., Ward, S., Burges, D., and Cooke, G. D. (1998) *Bacillus subtilis* ORF *yybQ* encodes a manganese-dependent inorganic pyrophosphatase with distinctive properties: the first of a new class of soluble pyrophosphatase? *Microbiology 144*, 2563−2571.
13. Shintani, T., Uchiumi, T., Yonezawa, T., Salminen, A., Baykov, A. A., Lahti, R., and Hachimori, A. (1998) Cloning and expression of a unique inorganic pyrophosphatase from *Bacillus subtilis*. Evidence for a new family of soluble inorganic pyrophosphatases, *FEBS Lett. 439*, 263−266.
14. Parfenyev, A. N., Salminen, A., Halonen, P., Hachimori, A., Baykov, A., and Lahti, R. (2001) Quaternary structure and metal-ion requirement of family II pyrophosphatases from *Bacillus subtilis*, *Streptococcus gordonii* and *Streptococcus mutans*, *J. Biol. Chem. 276*, 24511−24518.
15. Merckel, M. C., Fabrichniy, I. P., Salminen, A., Kalkkinen, N., Baykov, A. A., Lahti, R., and Goldman A (2001) Crystal structure of *Streptococcus mutans* pyrophosphatase: a new fold for an old mechanism, *Structure 9*, 289−297.
16. Ahn, S., Milner, A. J., Fütterer, K., Konopka, M., Ilias, M., Young, T. W., and White S. A. (2001) The "open" and "closed" structures of the type-C inorganic pyrophosphatases from *Bacillus subtilis* and *Streptococcus gordonii*, *J. Mol. Biol. 313*, 797−811.
17. Heikinheimo, P., Lehtonen, J., Baykov, A., Lahti, R., Cooperman, B. S., and Goldman, A. (1996). The structural basis for pyrophosphatase catalysis, *Structure 4*, 1491−1508.
18. DeLano, W. L. (2002) *The PyMOL Molecular Graphics System*, DeLano Scientific, San Carlos, CA.
19. Bradford, M. M. (1976) A rapid and sensitive method for the quantitation of microgram quantities of protein utilizing the principle of protein-dye binding, *Anal. Biochem. 72*, 248−254.
20. Chervenka, C. H. (1972) *Methods for the Analytical Ultracentrifuge*, Spinco Division of Beckman Instruments, Inc., Palo Alto, CA, 23−33.
21. Baykov, A. A., and Avaeva, S. M. (1981) A simple and sensitive apparatus for continuous monitoring of orthophosphate in the presence of acid-labile compounds, *Anal. Biochem. 116*, 1−4.
22. Conejero-Lara, F., Sanchez-Ruiz, J. M., Mateo, P. L., Burgos, F. J., Vendrell, J., and Aviles, F. X. (1991) Differential scanning calorimetric study of carboxypeptidase B, procarboxypeptidase B and its globular activation domain, *Eur. J. Biochem. 200*, 663−670.
23. Potekhin, S. A., Loseva, O., Tiktopulo, E. I., and Dobritsa, A. P. (1999) Transition state of the rate-limiting step of heat denaturation of Cry3A δ-endotoxin, *Biochemistry 38*, 4121−4127.
24. Baptista, R. P., Chen, L. Y., Paixao, A., Cabral, J. M. S., and Melo, E. P. (2003) A novel pathway to enzyme deactivation: The cutinase model, *Biotech. Bioeng. 82*, 851−857.
25. Dial, R., Sun, Z.-Y. J., and Freedman, S. J. (2003) Three conformational states of the p300 CH1 domain define its functional properties, *Biochemistry 42*, 9937−9945.
26. Mitkevich, V. A., Schulga, A. A., Ermolyuk, Y. S., Lobachov, V. M., Chekhov, V. O., Yakovlev, G. I., Hartley, R. W., Pace, C. N., Kirpichnikov, M. P., Makarov, A. A (2003) Thermodynamics of denaturation of complexes of barnase and binase with barstar, *Biophys. Chem. 105*, 383−390.
27. Wohlfahrt, G., Pellikka, T., Boer, H., Teeri, T., Koivula, A. (2003)-Probing pH-dependent functional elements in proteins: Modification of carboxylic acid pairs in *Trichoderma reesei* cellobiohydrolase Cel6A, *Biochemistry 42*, 10095−10103.
28. Zyryanov, A. B., Tammenkoski, M., Salminen, A., Kolomiytseva, G. Ya., Fabrichniy, I. P., Goldman, A., Lahti, R., and Baykov, A. A. (2004) Site-specific effects of zinc on the activity of family II pyrophosphatase, *Biochemistry 43*, 14395−14402.
29. Hyytiä, T., Halonen, P., Salminen, A., Goldman, A., Lahti, R., and Cooperman, B. S. (2001) Ligand binding sites in *Escherichia coli* inorganic pyrophosphatase. Effects of active site mutations, *Biochemistry 40*, 4645−4653.
30. Pohjanjoki, P., Fabrichniy, I. P., Kasho, V. N., Cooperman, B. S., Goldman, A., Baykov, A. A., and Lahti, R. (2001) Probing essential water in yeast pyrophosphatase by directed mutagenesis and fluoride inhibition measurements, *J. Biol. Chem. 276*, 434−441.
31. Fabrichniy, I. P., Lehtiö, L., Salminen, A., Zyryanov, A. B., Baykov, A. A., Lahti, R., and Goldman, A. (2004) Structural studies of metal ions in family II pyrophosphatases: The requirement for a Janus ion, *Biochemistry 43*, 14403−14411.
32. Koonin, E. V., and Tatusov, R. L. (1994) Computer analysis of bacterial haloacid dehalogenases defines a large superfamily of hydrolases with diverse specificity. Application of an iterative approach to database search, *J. Mol. Biol. 244*, 125−132.
33. Aravind, L., and Koonin, E. V. (1998) A novel family of predicted phoshoesterases includes *Drosophila* prune protein and bacterial RecJ exonuclease, *TIBS 23*, 17−19.
34. Yamagata, A., Kakuta, Y., Masui, R., and Fukuyama, K. (2002) The crystal structure of exonuclease RecJ bound to Mn^{2+} ion suggests how its characteristic motifs are involved in exonuclease activity, *Proc. Natl. Acad. Sci. U.S.A. 99*, 5908−5912.

BI047926U